Accessing the Triplet Manifold of Naphthalenebenzimidizole-Phenanthroline in Rhenium(I) Bichromophores

Journal:	*Dalton Transactions*
Manuscript ID	DT-ART-07-2021-002329.R1
Article Type:	Paper
Date Submitted by the Author:	06-Aug-2021
Complete List of Authors:	Wells, Kaylee ; North Carolina State University, Department of Chemistry Yarnell, James; North Carolina State University, Department of Chemistry Sheykhi, Sara; North Carolina State University, Department of Chemistry Palmer, Jonathan; North Carolina State University, Department of Chemistry Yonemoto, Daniel; North Carolina State University, Chemistry Joyce, Rosalynd; North Carolina State University, Department of Chemistry Garakyaraghi, Sofia; North Carolina State University, Chemistry Castellano, Felix; North Carolina State University, Department of Chemistry

ARTICLE

Accessing the Triplet Manifold of Naphthalenebenzimidizole-Phenanthroline in Rhenium(I) Bichromophores

Received 00th January 20xx,
Accepted 00th January 20xx

DOI: 10.1039/x0xx00000x

Kaylee A. Wells,*[a] James E. Yarnell, [a,b] Sara Sheykhi, [a] Jonathan R. Palmer, [a] Daniel T. Yonemoto, [a] Rosalynd Joyce, [a] Sofia Garakyaraghi,[a] and Felix N. Castellano [a]

The steady-state and ultrafast to suprananosecond excited state dynamics of *fac*-[Re(NBI-phen)(CO)$_3$(L)](PF$_6$)) (NBI-phen = 16H-benzo[4',5']isoquinolino[2',1':1,2]imidazo[4,5-f][1,10]phenanthrolin-16-one) as well as their respective models of the general molecular formula [Re(phen)(CO)$_3$(L)](PF$_6$) (L = PPh$_3$ and CH$_3$CN) were investigated using transient absorption and time-gated photoluminescnce spectroscopy. The **NBI-phen** containing molecules exhibited enhanced visible light absorption with respect to their models and rapid formation (< 6 ns) of the triplet ligand-centred (LC) excited state of the organic ligand, NBI-phen. These triplet states exhibit an extended excited state lifetime that enable the energized molecules to readily engage in triplet-triplet annhiliation photochemistry.

Introduction

Since Wrighton and co-workers original study,[1] rhenium(I) carbonyl diimine (Re-CDI) molecules have remained popular due to their thermal and photochemical stability, expansive photophysical properties, and ease of synthesis.[2-9] The synthetic flexibility of this class of chromophores allows for the molecule to be incorporated into polymers and supramolecular structures enabling a myriad of applications.[10-14] In fact, Re-CDI molecules are currently utilized in CO$_2$ reduction photochemistry, photochemical molecular devices, solar energy conversion, biological applications, and as sensors and photosensitizers.[15-24]

A significant drawback to many Re-CDI complexes is that they typically exhibit poor visible absorption properties and short triplet metal-to-ligand-charge-transfer (MLCT) lifetimes on the order of 100s of nanoseconds.[25] However, fine-tuning the electronic structure, and thus the corresponding electronic transitions, may be achieved through facile synthetic manipulations. The Re(I) dπ orbital energies are easily modified by varying the π-accepting and π-donating strength of the ancillary ligand, which are typically associated with the HOMO energy in these complexes.[26] Additionally, the π* orbital energies, the orbitals typically associated with the LUMO energy of the chromophoric diimine ligand, may also be adjusted by adding substituents on the diimine aromatic rings.[1] Thus, modification of both the ancillary and diimine ligands causes variations in the Re(I) dπ and diimine π* orbital energies, thereby modulating the MLCT excited state properties.

Our research group has conducted numerous studies monitoring changes in the excited state dynamics in Re-CDIs.[27-29] In these studies, we focused on appending additional organic chromophores within the ligand framework, which leads to excited state lifetime extension via a thermal equilibrium between the triplet ligand-centred (^{3}LC) and ^{3}MLCT excited states.[30-38] After extensively studying the photophysical interactions in these systems by modulation of both LC and MLCT excited state energies, we became interested in exploring new families of organic chromophores to determine what changes in their excited state dynamics might occur while testing their utility as light-harvesters and other potentially bespoke photophysical processes.

Most recently, we have investigated a series of thionated perinones[39] that exhibit efficient triplet excited state formation, building off work by Anzenbacher and co-workers on the oxygenated analogues.[40] Their work on polycyclic benzimidazoles inspired us to incorporate the perinone unit into rhenium(I) MLCT chromophores to increase their visible-absorption cross-sections and determine if the perinone triplet could be sensitized through the heavy-atom effect. Perinones are polycyclic aromatic hydrocarbons that belong to a class of organic dyes that have found extensive use in the automotive industry and in organic n-type semiconductor materials.[40-44] Considering their relatively high fluorescence quantum yields and significant visible absorption cross-sections, we postulated that this class of molecules would be of interest to construct newly conceived metal-organic bichromophores. Using the synthesis provided by Yang et al[45] to synthesize a perinone that is nested within a chelating ligand, we were able to successfully synthesize and photophysically characterize two new rhenium(I) bichromophores (**Chart 1**), *fac*-[Re(NBI-phen)(CO)$_3$(PPh$_3$)](PF$_6$) (**Re1**) and *fac*-[Re(NBI-

---

[a] *Department of Chemistry, North Carolina State University, Raleigh, North Carolina, 27695-8204, USA. E-mail: fncastel@ncsu.edu*

[b] *Department of Chemistry & Chemistry Research Center, United States Air Force Academy, Colorado Springs, Colorado, 80840-6230, United States*

†Electronic Supplementary Information (ESI) available: [Synthetic details and structural characterization data, and additional electronic theory calculations and spectroscopic data]. See DOI: 10.1039/x0xx00000x

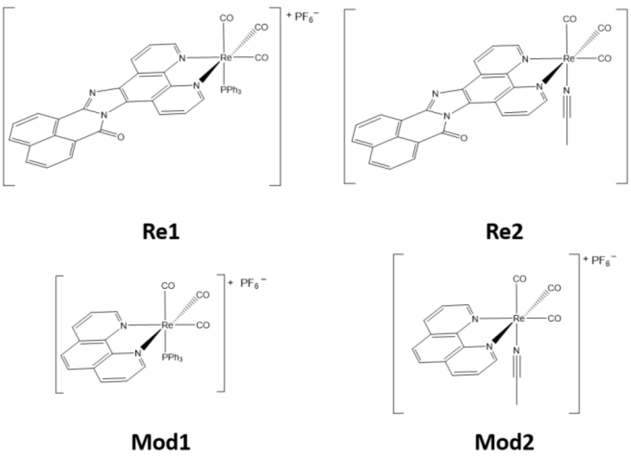

Chart 1. The bichromophores **Re1**, **Re2**, and relevant model complexes **Mod1**, and **Mod2** investigated here.

phen)$(CO)_3(CH_3CN)](PF_6)$ (**Re2**) (NBI-phen = naphthalene benzimidizole phenanthroline) as well as two model rhenium(I) chromophores *fac*-[Re(phen)$(CO)_3(PPh_3)](PF_6)$ (**Mod1**) and *fac*-[Re(phen)$(CO)_3(CH_3CN)](PF_6)$ (**Mod2**) which serve as control/model molecules to make direct comparisons to the bichromophores. The CH_3CN and PPh_3 moieties were purposefully selected as strong ancillary ligands to promote the formation of ligand-centered triplet excited states. Using a combination of steady-state and time-resolved techniques supported with computational modelling, we determined the **NBI-phen** ligand establishes the necessary energetics to serve as a visible light harvester featuring rapid formation of the long-lived ^{3}LC excited state.

Experimental

Reagents and Chemicals

All reagents and chemicals were purchased from Sigma—Aldrich or VWR and used as received. All syntheses were performed under an inert nitrogen atmosphere using standard techniques for the rigorous exclusion of air and water. Spectroscopic samples were prepared using spectroscopic-grade tetrahydrofuran and were prepared under an inert and dry atmosphere of nitrogen in a glovebox (MBraun). Complete synthesis and structural characterization details for all molecules investigated here are provided as ESI.

General Techniques

All chemicals and solvents were analytical grade, and they were used without further purification. Nuclear magnetic resonance (NMR) spectra were measured at 298 K with a Bruker® Avance NEO 700 MHz (^{1}H) and 176 MHz (^{13}C) and processed with MestreNova software (version 10.0.2), with the chemical shifts referenced to residual solvent signals. The chemical shifts (δ ppm) are referenced to the respective solvent, and splitting patterns are designated as s (singlet), d (doublet), t (triplet), m (multiplet). High resolution electrospray ionization mass spectrometry (HR-ESI-MS) was measured by the Michigan State University Mass Spectrometry Core, East Lansing, MI. MS values are given as m/z. Electronic absorption spectra was measured with a Shimadzu UV-3600 and Cary 60 UV/Vis spectrophotometer. Steady-state photoluminescence (PL) spectra and quantum yield measurements were measured on an Edinburgh FS 5 fluorimeter equipped with an integrating sphere (absolute). Excitation scans were performed on an Edinburgh FS 920 fluorimeter. All spectral PL measurements were performed using optically dilute samples at (0.1 ≥ OD) at excitation wavelength.

Characterization Data for Studied Molecules

16H-benzo[4',5']isoquinolino[2',1':1,2]imidazo[4,5-f][1,10]phenanthrolin-16-one (**NBI-phen**). (64 %). ^{1}H NMR (700 MHz, $CDCl_3$) δ 10.80 (d, *J* = 8.7 Hz, 1H), 9.56 (d, *J* = 8.2 Hz, 1H), 9.36 (t, *J* = 5.3 Hz, 2H), 9.23 (d, *J* = 7.4 Hz, 1H), 9.17 (d, *J* = 7.4 Hz, 1H), 8.66 (d, *J* = 8.1 Hz, 1H), 8.59 (d, *J* = 8.2 Hz, 1H), 8.45 – 8.42 (m, 1H), 8.33 – 8.30 (m, 1H), 8.14 (dd, *J* = 11.4, 4.0 Hz, 1H), 8.11 (t, *J* = 7.8 Hz, 1H) ppm. ^{13}C NMR (176 MHz, $CDCl_3$) δ 159.93, 151.64, 150.36, 144.93, 144.89, 139.16, 137.70, 137.44, 136.74, 135.76, 132.63, 132.25, 131.90, 129.08, 128.83, 128.02, 126.77, 126.29, 123.99, 121.76, 121.09, 120.94, 77.34, 77.16, 76.98, 21.26 ppm. MS [HR-ESI]: m/z calcd for $C_{24}H_{12}N_4OH$ $[M+H]^+$ 373.1089, found 373.1094. (**Fig. S1-3**).

fac-[Re(NBI-phen)$(CO)_3(PPh_3)](PF_6)$ (**Re1**).) (96 %). ^{1}H NMR (700 MHz, DMSO) δ 10.16 (d, *J* = 8.6 Hz, 1H), 9.41 (d, *J* = 5.0 Hz, 1H), 9.31 (t, *J* = 7.0 Hz, 2H), 8.97 (d, *J* = 7.1 Hz, 1H), 8.93 (d, *J* = 7.2 Hz, 1H), 8.69 (d, *J* = 8.0 Hz, 1H), 8.53 (d, *J* = 8.1 Hz, 1H), 8.09 (t, *J* = 7.6 Hz, 1H), 8.07 – 8.00 (m, 3H), 7.35 (t, *J* = 7.4 Hz, 3H), 7.25 (t, *J* = 6.7 Hz, 6H), 7.01 – 6.97 (m, 6H) ppm. ^{13}C NMR (176 MHz, DMSO) δ 194.95, 160.86, 155.04, 153.32, 152.42, 144.99, 144.44, 138.65, 138.32, 136.42, 134.14, 132.98, 132.86, 132.26, 132.20, 131.67, 131.05, 129.93, 129.13, 129.07, 128.08, 128.00, 127.82, 127.59, 127.50, 126.12, 125.99, 124.97, 124.47, 122.94, 122.59, 120.12, 40.02, 39.88, 39.76, 39.64, 39.52, 39.40, 39.28, 39.16 ppm. MS [HR-ESI]: m/z calcd for $C_{45}H_{27}N_4O_4PRe$ $[M]^+$ 903.1299, found 903.1307. (**Fig. S4-6**).

fac-[Re(NBI-phen)$(CO)_3(CH_3CN)](PF_6)$ (**Re2**). (71 %). ^{1}H NMR (700 MHz, CD_3CN) δ 10.48 (d, *J* = 8.6 Hz, 1H), 9.51 (t, *J* = 5.8 Hz, 2H), 9.47 (d, *J* = 4.8 Hz, 1H), 9.01 (d, *J* = 7.2 Hz, 1H), 8.96 (d, *J* = 7.2 Hz, 1H), 8.57 (d, *J* = 8.0 Hz, 1H), 8.42 (d, *J* = 8.1 Hz, 1H), 8.20 (ddd, *J* = 18.7, 8.4, 4.9 Hz, 2H), 8.01 (dt, *J* = 15.5, 7.7 Hz, 2H) ppm. ^{13}C NMR (176 MHz, CD_3CN) δ 155.38, 153.88, 146.88, 140.41, 140.10, 137.58, 135.93, 134.30, 133.87, 132.96, 128.94, 128.82, 128.67, 128.11, 127.30, 127.00, 126.49, 126.28, 124.40, 123.87, 123.48, 121.29, 120.71, 118.26, 68.24, 26.20, 1.27, 1.15. MS [HR-ESI]: m/z calcd for $C_{29}H_{15}N_5O_4Re$ $[M]^+$ 682.0654, found 682.0661. (**Fig. S7-9**).

fac-[Re(phen)$(CO)_3(PPh_3)](PF_6)$ (**Mod1**). (98 %). ^{1}H NMR (700 MHz, CD_3CN) δ 9.11 (dd, *J* = 5.1, 0.6 Hz, 2H), 8.62 (d, *J* = 8.2 Hz, 2H), 8.05 (s, 2H), 7.73 (dd, *J* = 8.2, 5.1 Hz, 2H), 7.33 (dt, *J* = 7.4, 3.7 Hz, 3H), 7.20 (td, *J* = 7.7, 2.1 Hz, 6H), 7.04 – 7.00 (m, 6H) ppm. ^{13}C NMR (176 MHz, CD_3CN) δ 155.79, 147.18, 140.24, 133.51, 133.45, 131.95, 131.93, 129.94, 129.88, 129.65, 129.38, 128.87, 127.56, 118.26, 1.27 ppm. MS [HR-ESI]: m/z calcd for $C_{33}H_{23}N_2O_3PRe$ $[M]^+$ 711.0976, found 711.0970. (**Fig. S10-12**).

fac-[Re(phen)$(CO)_3(CH_3CN)$](PF_6) (**Mod2**). (91 %). ^{1}H NMR (400 MHz, CD_2Cl_2) δ 9.38 (dd, *J* = 5.1, 1.3 Hz, 2H), 8.80 (dd, *J* = 8.3, 1.3 Hz, 2H), 8.21 (s, 2H), 8.05 (dd, *J* = 8.3, 5.1 Hz, 2H), 2.06 (s, 3H), 1.54 (s, 3H) ppm. ^{13}C NMR (176 MHz, CD_2Cl_2) δ 154.46, 147.24, 140.55, 131.72, 128.63, 127.13, 54.15, 54.00, 53.84, 53.69, 53.53, 3.70 ppm. MS [HR-ESI]: m/z calcd for $C_{17}H_{11}N_3O_3Re$ $[M]^+$ 490.0330, found 490.0339. (**Fig. S13-15**).

Ultrafast Transient Absorption Spectroscopy

The transient absorption measurements were performed at the NCSU Imaging and Kinetic Spectroscopy (IMAKS) Laboratory using a mode-locked Ti:sapphire laser (Coherent Libra) as described previously.[46] The pump beam was directed into a parametric amplifier (Coherent OPerA Solo) to generate the 400 nm excitation. The probe beam was focused onto a calcium fluoride crystal to generate a white light continuum between 350 and 750 nm. The pump beam (~700 µm) was focused and overlapped with the probe beam through a 2 mm path length cuvette to allow for a stir bar to be used. The ground-state absorption spectra were taken before and after each experiment to ensure there was no sample photo-degradation during the experiment. The transient kinetic data at specific wavelengths was evaluated using the fitting routines available in OriginPro 2018b (v 9.55).

Nanosecond Transient Absorption and Time—Resolved Photoluminescence Spectroscopy

Nanosecond transient absorption (nsTA) and time—resolved photoluminescence (TR—PL) measurements were collected with a LP920 laser flash photolysis system from Edinburgh Instruments controlled by L900 software program (Edinburgh Instruments). A Vibrant 355 Nd:YAG/OPO system (OPOTEK) was used for pulsed laser excitation for **Re1** and **Re2**. A Continuum Minilite Nd:YAG laser with 355 nm excitation was used for pulsed laser excitation for **Mod1** and **Mod2**. To collect the transient absorption difference spectra and time—gated PL spectra in the visible portion of the spectrum, an iStar ICCD camera (Andor Technology), controlled by L900 was used. Single—wavelength kinetic analysis for absorption and PL were collected using a R2658P PMT detector (Hamamatsu) also controlled by L900. Samples were prepared under an inert and dry atmosphere of nitrogen in a glovebox (MBraun) in a 10 mm path-length quartz optical cell. Samples were prepared to have optical densities between 0.3 and 0.6 at the excitation wavelength (λ_{ex} = 410 nm for **Re1** and **Re2** and λ_{ex} = 355 nm for **Mod1** and **Mod2**). All flash-photolysis experiments were performed at room temperature unless otherwise noted. The ground-state electronic absorption spectra were recorded before and after each experiment to ensure no sample photo-degradation. The transient kinetic data was evaluated using the fitting routines available in Origin Student 2018b (v. 9.55).

Density Functional Theory (DFT) and Time—Dependent DFT (TD-DFT) Calculations

Density functional theory (DFT) and time-dependent DFT (TD-DFT) calculations were performed on all complexes using the Gaussian 16 software package (revision A.03)[47] and the computational resources of the North Carolina State University High Performance Computing Center. Geometry optimizations and TD-DFT calculations were performed using the PBE1PBE

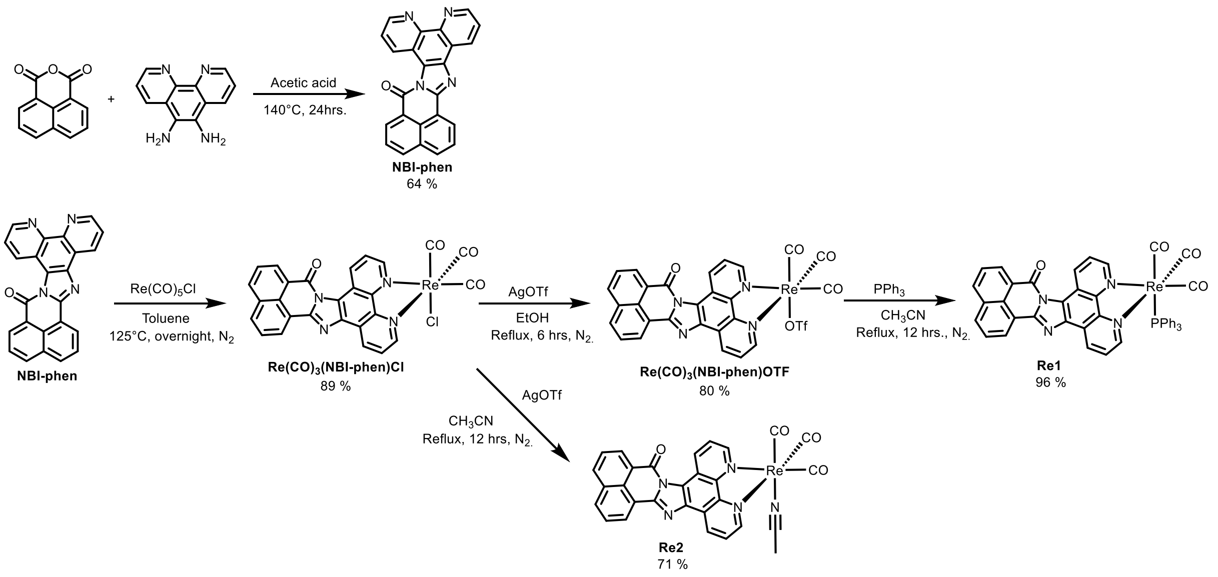

Scheme 1. Synthetic pathways leading to **NBI-phen**, **Re1**, and **Re2**.

(PBE0) functional[48] and the Def2-SVP basis set of the Alrichs group on all atoms.[49] The Stuttgart-Dresden effective core potentials (ECP) were used to replace the core electrons in rhenium for all calculations.[50] The polarizable continuum model (PCM)[51] was used to simulate the effects of the tetrahydrofuran (THF) solvent environment for all calculations, and the GD3 dispersion correction[52] was used for all ground and excited state geometry optimizations. Frequency calculations were performed on all optimized structures and no imaginary frequencies were obtained. TD-DFT calculations were used to obtain the energy, oscillator strength, and related molecular orbital contributions for the 50 lowest singlet-singlet vertical transitions for all molecules studied. The natural transition orbitals (NTOs)[53] of the low-lying singlet-singlet transitions were generated and visualized using GaussView 6.0.[54] Triplet spin density surfaces and natural orbitals (NOs) were generated from the optimized T_1 excited states and were also visualized with GaussView 6.0.

Results and discussion

Syntheses

All syntheses were performed under an inert and dry nitrogen atmosphere using standard techniques. All reagents were purchased from VWR or Sigma-Aldrich and used as received. The synthetic procedures used to make all the chromophores are outlined in Scheme 1. The identity and purity of all compounds studied were confirmed using ^{1}H NMR, ^{13}C NMR, and high-resolution mass spectrometry. Synthetic details for all precursors and products in this study are included in the Supporting Information. Briefly, 1,8-naphthalic anhydride, 5,6-diamino-1,10-phenanthroline, and acetic acid were added to a pressure vessel and heated to 140 °C for 24 hours to synthesize the **NBI-phen** ligand.[45] Synthesis of **Re1** and **Re2** began with **NBI-phen** and $Re(CO)_5Cl$ refluxing in toluene to make the chloride intermediate. **Re1** was then treated with AgOTf in EtOH to remove the chloride which was then reacted with PPh_3 in CH_3CN to synthesize the final product. **Re2** also began with the chloride intermediate as with **Re1** but was treated with AgOTf in CH_3CN to synthesize the final product. **Mod1** and **Mod2** were synthesized according to previous literature precedence.[55, 56]

Electronic Structure Calculations

Ground state geometry optimizations were initially performed on both the model complexes (**Mod1** and **Mod2**) and the bichromophores (**Re1** and **Re2**) to establish how the frontier molecular orbitals are altered by interchanging 1,10-phenanthroline with **NBI-phen** as the diimine ligand. Representative frontier orbital diagrams are shown below in **Figure 1** for **Mod1** and **Re1**. Corresponding diagrams are reported in **Figure S16** for **Mod2** and **Re2**. The frontier orbitals for **Mod1** depict the three highest occupied molecular orbitals to be the Re(I) dπ orbitals, while the LUMO corresponds to the π* orbital on the diimine. This suggests that the lowest energy transitions in the UV-Vis of this complex are MLCT in nature. Similar conclusions can be drawn from **Figure S16** for **Mod2**. Conversely, the frontier orbitals for **Re1** reveal the emergence of a diimine-based π molecular orbital as the HOMO, while the

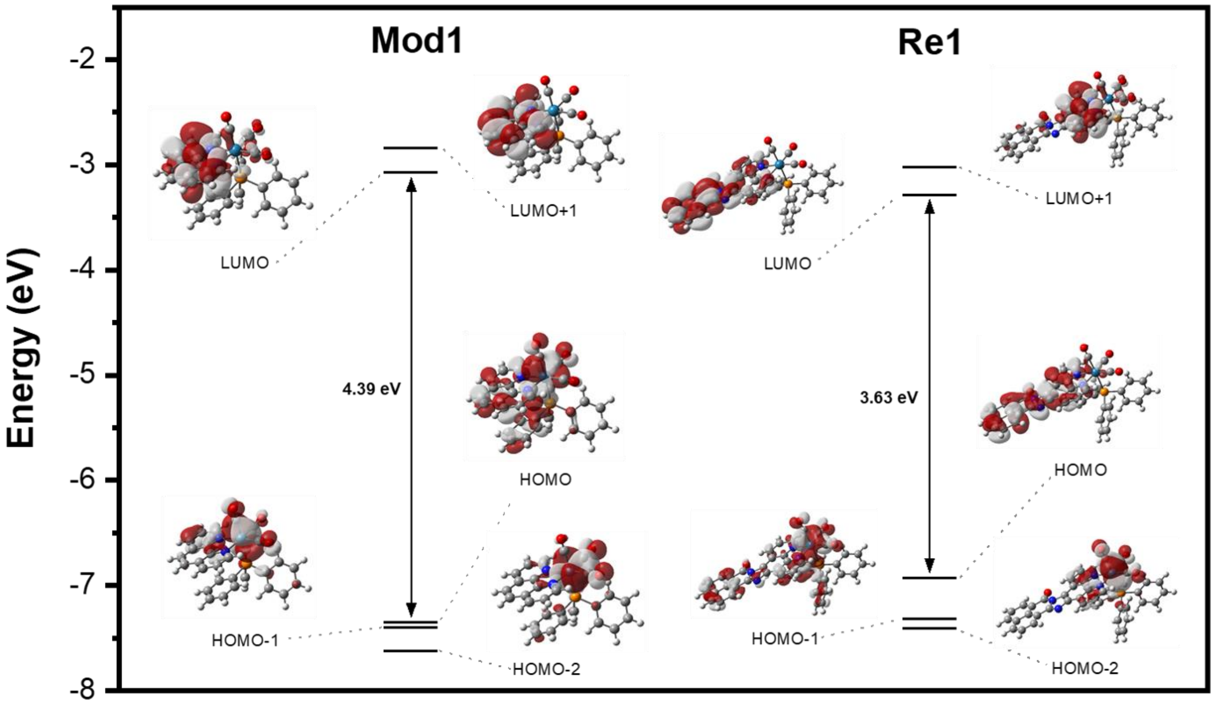

Figure 1. Representative frontier molecular orbital diagrams of the **Mod1** and corresponding NBI-phen complex **Re1**, where L = PPh_3.

LUMO is lowered in energy and maintained as the π^* orbital on the diimine. Additionally, the HOMO-LUMO gap is calculated to be much smaller in **Re1** than in **Mod1** (~0.6 eV). As a result, it is expected that the lowest energy transition in **Re1** is ligand-centered and the complex will exhibit superior visible light absorption than its corresponding model complex, **Mod1**. Similarly, this trend is also observed when comparing **Mod2** to **Re2**.

Using the optimized ground state geometries, the electronic absorption spectrum of each complex was simulated by calculating the 50 lowest singlet transitions for each complex. The calculated electronic absorption spectra of **Mod1** and **Re1** are presented in **Figures S17** and **S18**, respectively, and are overlaid with their experimental spectra. For **Mod1**, the calculated spectrum is in good agreement with experimental data, with the lowest energy absorption maximum being slightly overestimated in energy. The calculated electronic absorption spectrum of **Re1** is also in good agreement with experimental data, with the lowest energy absorption maximum being slightly underestimated in energy. Natural transition orbitals were calculated for the three lowest-lying vertical excitations of **Mod1** and **Re1** to elucidate the character of the transitions making up the majority of the lowest energy absorption bands. The resultant hole-particle pairs are displayed in **Figure S21** for **Mod1** and **Figure S22** for **Re1**. The energies and oscillator strengths for these transitions are compiled in **Table S1**. The three lowest energy singlet transitions for **Mod1** are all MLCT in nature with low oscillator strength. The hole corresponds to a Re(I) dπ orbital in each case and the particle corresponds to a π^* orbital on the diimine. Conversely, the lowest energy singlet transition for **Re1** is LC in nature with significant oscillator strength. The hole corresponds to a π orbital on the diimine and the particle corresponds to a π^* orbital on the diimine. The pure MLCT transition for **Re1** is not observed until the $S_0 \rightarrow S_3$ transition, which is significantly higher in energy with much lower oscillator strength than the LC transition (see **Table S1**). These results are consistent with those predicted from the change in frontier molecular orbitals shown in **Figure 1** when interchanging 1,10-phenanthroline with **NBI-phen** as the diimine, and is also observed in **Mod2** and **Re2** (**Figures S23-24)**.

The character of the lowest energy triplet excited state in the bichromophores were assigned by calculating natural orbitals from the optimized geometry of the lowest energy triplet state. Using **Re1** as a representative example, the singly-occupied natural orbitals display the unpaired spins to be located on the diimine ligand in orbitals of π-symmetry (**Figure S25**). It should be noted that the natural orbitals depict a significant degree of intra-ligand charge transfer in this triplet excited state, which is not observed in the lowest energy singlet vertical LC transition predicted using TD-DFT. Additionally, the Re(I) dπ natural orbitals are observed to all be doubly occupied, further confirming there is no MLCT character in this lowest energy triplet excited state. The natural orbital analysis for **Re2** depicted in **Figure S26** gives the same results. Finally, the spin density surfaces generated from the lowest energy triplet state of **Re1** and **Re2** both depict spin density to be localized solely on the **NBI-phen** ligand (**Figure S27**), corroborating that the lowest energy triplet excited state in these complexes are ^{3}LC.

Electronic Absorption and Photoluminescence Spectroscopy

The electronic absorption spectra of **Re1-2** and **Mod1-2** are presented in **Figure 2**, with additional spectroscopic results in **Table 1**. **Mod1** and **Mod2** are the model inorganic chromophores for this study and **NBI (Figure S29)** is used as a model organic chromophore. **NBI-phen** is not used as the organic model due to its insolubility in many organic solvents. During photophysical study of the two bichromophores (discussed below), **Re1** and **Re2**, it became clear that these molecules shared remarkably similar characteristics with the features seen in an Ir(III) chromophore featuring the **NBI** ligand.[57] While the photophysical data for **NBI** will be used in lieu of **NBI-phen**, it is important to note that due to the extended π system of **NBI-phen** a bathochromic shift in its absorption and photoluminescence features is expected.

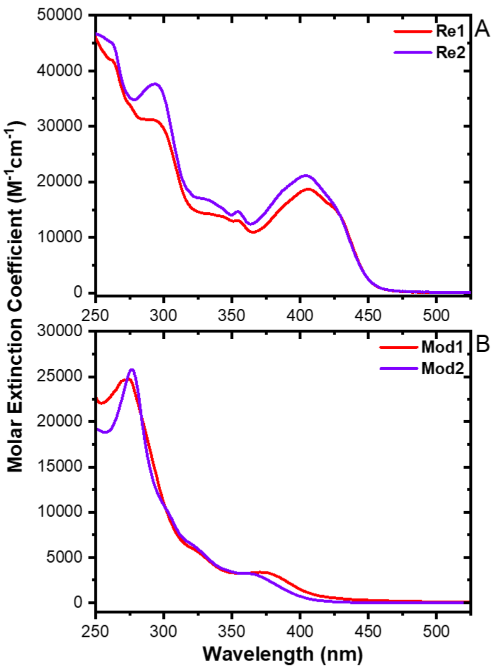

Figure 2. Electronic absorption spectra of (A) **Re1** and **Re2** and (B) **Mod1** and **Mod2** measured in THF.

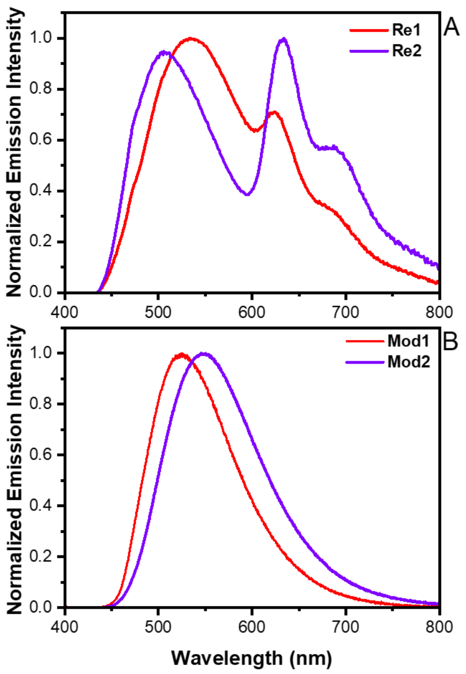

Figure 4. Static photoluminescence spectra of (A) **Re1** and **Re2** (λ_{ex} = 415 nm) and (B) **Mod1** and **Mod2** (λ_{ex} = 355 nm) in deaerated THF.

Table 1. Electronic absorbance and photoluminescence data of studied molecules in THF.

Molecule	λ_{abs}, nm (ε, M^{-1} cm^{-1})	λ_{am}, nm RT[a] (77 K)[b]	Φ_{em}[c] (%)
Re1	292 (31200)	535, 624, 688	< 1
	406 (18700)	(540, 614, 675)	
Re2	294 (37700)	506, 633, 689	< 1
	404 (21200)	(532, 615, 672)	
Mod1	275 (24700)	524	46.8
	374 (3340)		
Mod2	277 (25800)	548	11.7
	365 (3180)		

[a] Room temperature PL maxima are corrected and were performed in deaerated THF. [b] 77 K measurements were made with 2-MeTHF and PL maxima are uncorrected. [c] Absolute quantum yields.

From **Figure 2A**, the visible absorption cross-section was observed to be markedly enhanced for **Re1** and **Re2** as compared to their respective model chromophores, **Figure 2B**. This increase in visible light absorptivity is a direct consequence of the **NBI** being fused to the 1,10-phenanthroline ligand. The higher energy transitions of both **Re1** and **Re2** in the UV, < 300 nm, are of higher energy $\pi \rightarrow \pi^*$ transitions on the diimine ligand. The generally broad and slightly featured low energy band has a peak maximum at 406 nm with a shoulder at 425 nm for **Re1** and 404 nm with a shoulder at 425 nm for **Re2**. TD-DFT calculations of both **Re1** and **Re2** indicate the lowest energy transition, $S_0 \rightarrow S_1$, is a $\pi \rightarrow \pi^*$ transition localized on the **NBI-phen**. It is not until the $S_0 \rightarrow S_3$ transition that MLCT character is observed at much higher energy. **NBI**, **Figure S29**, has a largely broad and featureless low energy band. Computations show that the two lowest energy transitions are comprised of a charge transfer band where the electron density is localized along the π system of the entire ligand and then shifts towards the naphthalene end of the ligand ($S_0 \rightarrow S_1$) and a $\pi \rightarrow \pi^*$ transition ($S_0 \rightarrow S_2$).[39] This behaviour is mirrored in the **NBI-phen** ligand as seen in the computations (**Figure S28**).

The static PL spectra of **Re1** and **Re2** share similar features (**Figure 3A**) after being excited with 415 nm. **Re1** has three peak maximums at 535, 624, and 688 nm. The peak maximums of **Re2** are 506, 633, and 689 nm. The slight shoulder at 477 nm in both complexes is from the Raman band of THF which is noticeable due to the low quantum yield values for both bichromophoric complexes (< 1%). For both molecules, the highest energy peak is assigned to the singlet fluorescence of the organic chromophore due to their similar peak positions and because the peak remains even after being exposed to molecular dioxygen (**Figure S30**). The two lower energy features are therefore designated to be the triplet PL emission of the **NBI-phen** ligand, which were completely quenched by exposure to molecular dioxygen (**Figure S30**). Further evidence of these peaks triplet character is the triplet sensitized spectrum of **NBI** recorded by Yarnell and co-workers.[57] In their study, they found the triplet state of **NBI** to emit at 607 and 664 nm in 2-MeTHF. Excitation scans (**Figure S31**) monitoring emission intensity at all three observed PL peaks for both **Re1** and **Re2** reproduced the lowest energy band of the absorbance spectra that we characterize as exclusively **NBI-phen** electronic transitions. These combined data all suggest that not only do these molecules obey Kasha's rule, the lowest emitting state of these

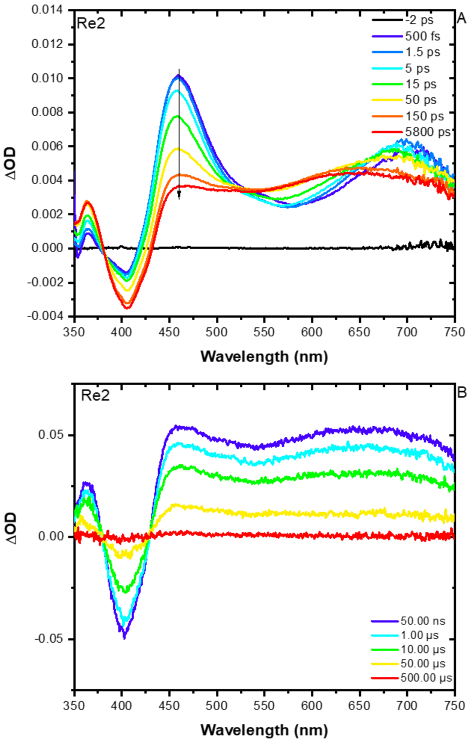

Figure 3. UFTA of (A) **Re2** in THF following 400 nm pulsed laser excitation (105 fs fwhm, 0.3 mJ/pulse) and (B) nsTA of **Re2** in deaerated THF following 415 nm excitation (1.8 mJ/pulse).

two bichromophores consists of triplet **NBI-phen** with residual singlet fluorescence of the same unit.

Mod1 and **Mod2** electronic absorption spectra are presented in **Figure 2B** and their steady-state PL in **Figure 3B**. The absorbance and photoluminescence spectra of both model compounds are analogous to previously synthesized rhenium(I) tricarbonyl diimines of similar structure.[2, 28, 29, 55, 56, 58] **Mod1** and **Mod2** absorption spectrum is characterized by strong UV absorption < 300 nm correlating to $\pi\rightarrow\pi^*$ transitions of the phenanthroline ligand. The lower energy band of the model complexes with peak maximums at 374 and 365 nm for **Mod1** and **Mod2** respectively are attributed to the MLCT transition, consistent with previously reported data of similarly constructed molecules and agree with the TD-DFT calculations performed (discussed above). The PL of both models (**Figure 3B**) are assigned to the ^{3}MLCT excited state due to their large stokes shift (524 nm, **Mod1**, and 548 nm, **Mod2**), broad and featureless profile, and excited state lifetime (discussed below). Additionally, previous molecules of a similar structural motif have their PL assigned to being ^{3}MLCT character.[2, 28, 29, 55, 56, 58]

Transient Absorption and Time—Resolved PL Spectroscopy

Ultrafast Transient Absorption Spectroscopy. The ultrafast excited state absorption difference spectra of **Re2** are presented in **Figure 4A**, and **Mod2** in **Figure 5A**, while those of **Re1** and **Mod1** are presented in **Figure S32A and S38A,** respectively. **Re2** ultrafast excited state difference spectra (**Figure 4A**) is used as representative data for both bichromophores as the UFTA of **Re1** is nearly identical. The UFTA of **Re2** shares similar features at early time scales with **NBI** (**Figure S37**). The prompt signal shows that there are excited state features that align well with **NBI** at 363, 460, and 698 nm. The dip in the excited state between 460 and 698 nm is due to stimulated emission that is not quite intense enough to be a negative feature but still distorts the excited state features at early time delays. Additionally, there is a ground state bleach centered at 406 nm, in good agreement with the low energy absorption band already assigned to ^{1}LC transitions within the **NBI-phen** unit (**Figure 2A**). Over the course of the experiment, the excited state features evolve into a state where there is no stimulated emission; the excited state features in the visible region peak at 460 nm and span out into the NIR. This behaviour is in stark contrast to **NBI** where no new features are seen after 6 ns (**Figure S37**).

Single wavelength analysis of **Re2** at 460 nm yields a biexponential decay where the faster time constant is 10.5 ps and the second is 74.2 ps (**Re1** τ_1 = 7.6 and τ_2 = 39.1 ps) (**Figures S33-34**). Due to the similar features between the prompt signal of the bichromophores and the **NBI**, we have attributed the first time constant to the singlet decay of the organic ligand on the bichromophores. The second time constant we are assigning to the ISC rate from the singlet manifold to the triplet manifold of the **NBI-phen** ligand. These two time constants are consistent with the work done by Blanco-Rodríguez et al where ISC from the singlet state to the triplet state is possible due to the close proximity of a heavy atom, rhenium.[59, 60] There is no spectroscopic or kinetic evidence that the MLCT-based electronic transitions play an active role in the ultrafast time domain of these molecules as seen in previous bichromophoric studies. However, there is spectroscopic evidence that the **NBI-phen** is entering its triplet excited state. The final trace at 6 ns in **Figure 4A** mimics the initial trace in the nsTA spectra in **Figure 4B**. Lack of new spectroscopic features between the two experiments implies that the final excited state is formed in the ultrafast and then decays back to ground state. Further evidence that supports assignment of ^{3}LC character of the **NBI-phen** as the final excited state is discussed immediately below.

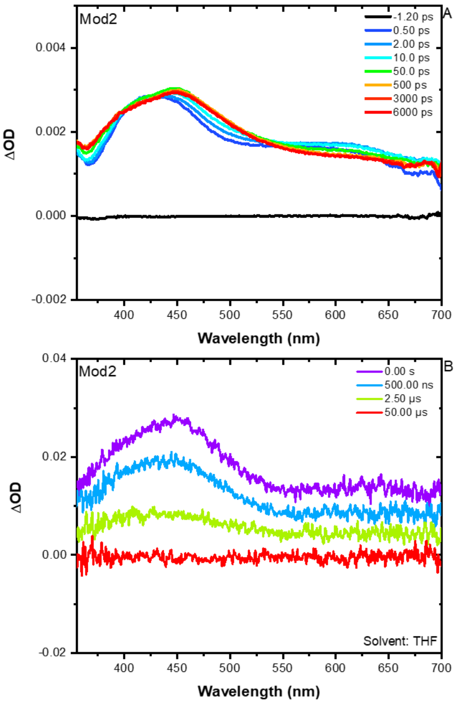

Figure 5. Representative (**Mod1** and **Mod2**) transient absorption spectra of (A) UFTA of **Mod2** following 350 nm excitation (105 fs fwhm, 50 μJ/pulse) in THF and (B) nsTA of **Mod2** following 355 nm excitation (1.8 mJ/pulse) in deaerated THF.

Representative ultrafast excited state difference spectra of the models are of **Mod2** are presented in **Figure 5A** (**Mod1 Figure S38A**). After 350 nm excitation (105 fs fwhm, 50 μJ/pulse), the compound displays only excited state features that develop a more refined shape over the course of the experiment with peak maxima at 400 and 450 nm. These absorption features are vastly different than their respective bichromophoric molecule (**Figure 4A, S32A**). The associated short time constants observed in **Mod1** and **Mod2** are significantly different (< 150 fs) than those measured in **Re1** and **Re2**. Additionally, the longer time decay components observed in the model complexes, 8.84 and 9.35 ps for **Mod2** and **Mod1** respectively, (**Figures S39-40**) are unique with respect to the kinetics observed in the title chromophores. The faster time constant measured for both models are assigned to intersystem crossing and formation of the radical anion on the diimine ligand. The longer time components are believed to correspond to vibrational cooling on the triplet surface. Both time constants are in good agreement with previously studied Re-CDI molecules featuring MLCT excited states.[5, 8, 28, 29]

Nanosecond Transient Absorption and Time-Gated PL. The nsTA excited state difference spectra of **Re2** is displayed in **Figure 4B** as representative data for both bichromophores of this study. From the trace, we see that the features are consistent with the final trace from the UFTA data indicating that the same excited state is observed at the end of the UFTA experiment and throughout the nsTA experiment. There are two excited state features, one in the UV ca. 375 nm and one that peaks in the visible near 460 nm that broadens out to the NIR. These two features sandwich a ground state bleach at 400 nm. Because both **Re1** and **Re2** have nearly identical excited state features and ground state bleaches, this suggests that the excited state observed in the ns time domain is of ^{3}**NBI-phen** as it is the shared ligand between the two compounds. Additionally, these features persist for hundreds of microseconds suggesting that the associated excited state observed is of ^{3}LC character. Further support that the excited state observed is ^{3}**NBI-phen** is the triplet sensitized nsTA spectrum of ^{3}**NBI** presented by Yarnell et. al where there is an excited state feature ca. 450 nm that spans out to the NIR.[57] This slight blue shift in the excited state difference spectrum is expected as the ligand is structured differently and is a free ligand in solution. Single-wavelength kinetic analysis at 460 nm yielded a kinetic trace that could not be fit to a mono-exponential decay and was found to be power dependent in nature. Observing this phenomenon, we fit the data using eq. 1

$$\Delta A = \frac{\Delta A_0(1-\beta)}{\exp(k_T t)-\beta} \qquad \text{eq. 1}$$

where β equates to the initial fraction of triplet decay occurring through TTA.[61]

From this fitting equation and multiple experimental pulse energies (**Figures S35-36, Tables S3-4**), we were able to ascertain that these molecules, **Re1** and **Re2**, undergo triplet-triplet annihilation (TTA) with themselves and have an experimental triplet decay rate constant on the order of 10^3 s^{-1}.

Room temperature and 77 K TR-PL spectra of **Re2** are displayed in **Figure 6** with relevant peak maximums in **Table 1**. In the RT experiment (**Figure 6A**) with a long gate (10.00 µs), we were able to resolve one feature at 515 with two red shoulders at 623, and 684 nm. Under similar experimental conditions **Re1** displayed a feature at 532 nm but only one shoulder at 622 nm (**Figure S41A**). In a frozen glass at 77 K, the red features became more pronounced, appearing much more like the features seen in the static PL spectra (**Figure 3A**). As such, we confidently assign the features as ^{1}LC and ^{3}LC in nature. Additionally, we were able to watch the RT PL decay over the same time range as the transient absorption (**Figure 4B**) experiment discussed above. The incredibly long-lived excited state, excited state spectral features, TR-PL, and calculations all lend significant support in assigning ^{3}**NBI-phen** as the final excited state.

Mod2 nsTA is displayed in **Figure 5B** and is representative of **Mod1** (**Figure S38B**). Upon 355 nm excitation, prompt signal shows positive absorption features across the entire visible region, similar to its UFTA, **Figure 5A**. The excited state features of both model complexes resemble the ^{3}MLCT transition in Re-CDI molecules featuring a phenanthroline ligand.[27-29, 62] Additionally, the lifetimes of the two models are consistent with $[Re(phen)(CO)_3(L)]^+$ (L = neutral ligand) molecules featuring a ^{3}MLCT with lifetimes of 2.2 and 2.3 µs for **Mod1** and **Mod2** respectively (**Figure S44-45**).[2, 28, 56] The TR-PL and their PL lifetimes of both models are presented in **Figure S42-45**. Like their steady-state PL, the TR-PL spectra of the models are broad and featureless with peak maxima at 516 nm and 540 nm for **Mod1** and **Mod2**, respectively. Over the course of the experiment, no new features are noted, and the experimental lifetime of their PL (τ = 2.5 µs for both **Mod1** and **Mod2**) matches their nsTA lifetime indicating that the final excited state is also the emitting state.

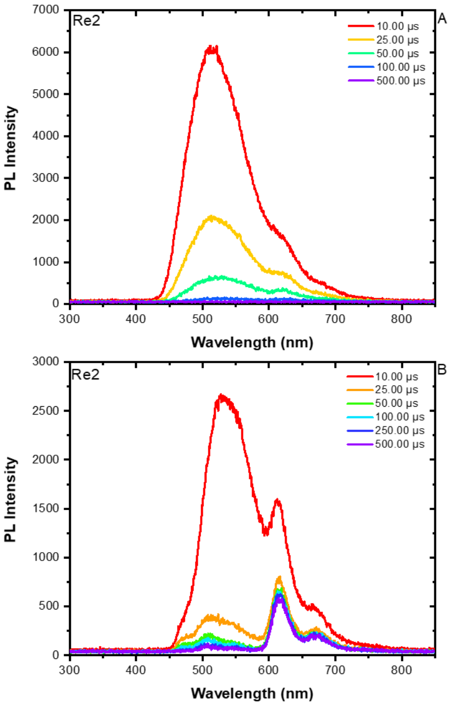

Figure 6. Representative (**Re1** and **Re2**) time-resolved photoluminescence data of **Re2** at (A) room temperature in deaerated THF and (B) 77 K in 2-MeTHF following 415 nm excitation (1.8 mJ/pulse).

Conclusions

In this study, we have successfully integrated a perinone, **NBI-phen**, onto two Re(I) carbonyl diimine complexes and have fully characterized the excited state processes from prompt excitation to ground state and compared them to their respective model compounds. Additionally, we have used electronic structure calculations to provide theoretical relevance and support for our experimental findings. This study has revealed that by integrating the **NBI-phen** ligand into the framework of the Re-CDI, we obtain higher visible light absorptivity and extended excited state lifetimes that are capable of self-quenching via TTA in solution. However, the incorporation of the perinone onto the Re(I) centre dramatically decreased the quantum yield. We conclude that upon excitation, the ^{1}LC band of the **NBI-phen** undergoes ISC to the ^{3}LC due to the heavy-atom effect presented by Re(I), where it then decays back to the ground state. Lastly, while a thermal equilibrium between the organic ligand and Re-CDI was not formed in these two systems due to the large energy gap between the ^{3}MLCT and ^{3}LC states, the long-lived nature of the **NBI-phen** ^{3}LC state makes these materials an ideal candidate as a low-lying triplet reservoir. As such, if an inorganic chromophore of appropriate MLCT energy is introduced in place of our present Re-CDI complexes, a strong thermal equilibrium is likely to establish.[27-38] However, these materials are well suited for light harvesting applications and readily sensitize the organic triplet making them good candidates for a variety of applications.[11, 13, 15-17, 24]

Author Contributions

KAW was involved in conceptualization, formal analysis, experimental investigation, validation, visualization, writing and editing the manuscript. JEY was involved in conceptualization and experimental investigation. SS was involved in experimental investigation and writing the original manuscript. JRP was involved in experimental investigation and editing the manuscript. DTY was involved in validation and editing the manuscript. RJ was involved in experimental investigation. SG was involved in experimental investigation. FNC was involved in conceptualization, funding acquisition, resources, visualization, and editing the manuscript.

Conflicts of interest

There are no conflicts of interest to declare.

Acknowledgements

This work was supported by the U.S. Department of Energy, Office of Science, Office of Basic Energy Sciences, under Award No. DE-SC0011979. Some personnel were supported by the National Science Foundation (CHE-1955795, K.A.W.), the Air Force Institute of Technology (AFIT, J.E.Y.), the Air Force Office of Scientific Research (FA9550-18-1-0331, D.T.Y.).

References

1. M. Wrighton and D. L. Morse, *J. Am. Chem. Soc.*, 1974, **96**, 998-1003.
2. L. Wallace and D. P. Rillema, *Inorg. Chem.*, 1993, **32**, 3836-3843.
3. S. A. Moya, J. Guerrero, R. Pastene, R. Sartori, R. Schmidt, R. Sariego, J. Sanz-Aparicio, I. Fonseca and M. Martinez-Ripoll, *Inorg. Chem.*, 1994, **33**, 2341-2346.
4. G. E. Shillito, T. B. J. Hall, D. Preston, P. Traber, L. Wu, K. E. A. Reynolds, R. Horvath, X. Z. Sun, N. T. Lucas, J. D. Crowley, M. W. George, S. Kupfer and K. C. Gordon, *J. Am. Chem. Soc.*, 2018, **140**, 4534-4542.
5. A. El Nahhas, C. Consani, A. M. Blanco-Rodríguez, K. M. Lancaster, O. Braem, A. Cannizzo, M. Towrie, I. P. Clark, S. Záliš, M. Chergui and A. Vlček, *Inorg. Chem.*, 2011, **50**, 2932-2943.
6. J. M. Villegas, S. R. Stoyanov, W. Huang and D. P. Rillema, *Inorg. Chem.,* 2005, **44**, 2297-2309.
7. J. L. Smithback, J. B. Helms, E. Schutte, S. M. Woessner and B. P. Sullivan, *Inorg. Chem.*, 2006, **45**, 2163-2174.
8. H. Atallah, C. M. Taliaferro, K. A. Wells and F. N. Castellano, *Dalton Trans.*, 2020, **49**, 11565-11576.
9. A. Vlček, in *Photophysics of Organometallics*, ed. A. J. Lees, Springer Berlin Heidelberg, Berlin, Heidelberg, 2010, DOI: 10.1007/3418_2009_4, pp. 115-158.
10. A. J. North, J. A. Karas, M. T. Ma, P. J. Blower, U. Ackermann, J. M. White and P. S. Donnelly, *Inorg. Chem.*, 2017, **56**, 9725-9741.
11. N. M. Orchanian, L. E. Hong, J. A. Skrainka, J. A. Esterhuizen, D. A. Popov and S. C. Marinescu, *ACS Appl. Energy Mater.*, 2019, **2**, 110-123.
12. M. A. Shestopalov, Y. V. Mironov, K. A. Brylev, S. G. Kozlova, V. E. Fedorov, H. Spies, H.-J. Pietzsch, H. Stephan, G. Geipel and G. Bernhard, *J. Am. Chem. Soc.*, 2007, **129**, 3714-3721.
13. M. Toganoh, S. Ikeda and H. Furuta, *Inorg. Chem.*, 2007, **46**, 10003-10015.
14. O. A. Nikonova, K. Jansson, V. G. Kessler, M. Sundberg, A. I. Baranov, A. V. Shevelkov, D. V. Drobot and G. A. Seisenbaeva, *Inorg. Chem.*, 2008, **47**, 1295-1300.
15. F. Franco, C. Cometto, C. Garino, C. Minero, F. Sordello, C. Nervi and R. Gobetto, *Eur. J. Inorg. Chem.* , 2015, **2015**, 296-304.
16. J. Agarwal, E. Fujita, H. F. Schaefer and J. T. Muckerman, *J. Am. Chem. Soc.*, 2012, **134**, 5180-5186.
17. H. Takeda, K. Koike, H. Inoue and O. Ishitani, *J. Am. Chem. Soc.*, 2008, **130**, 2023-2031.
18. K. P. S. Zanoni and N. Y. Murakami Iha, *Dalton Trans.*, 2017, **46**, 9951-9958.
19. A. O. T. Patrocinio, K. P. M. Frin and N. Y. Murakami Iha, *Inorg. Chem.*, 2013, **52**, 5889-5896.
20. K. M. Knopf, B. L. Murphy, S. N. MacMillan, J. M. Baskin, M. P. Barr, E. Boros and J. J. Wilson, *J. Am. Chem. Soc.*, 2017, **139**, 14302-14314.
21. M. A. Klenner, B. Zhang, G. Ciancaleoni, J. K. Howard, H. E. Maynard-Casely, J. K. Clegg, M. Massi, B. H. Fraser and G. Pascali, *RSC Advances*, 2020, **10**, 8853-8865.
22. L. C.-C. Lee, K.-K. Leung and K. K.-W. Lo, *Dalton Trans.*, 2017, **46**, 16357-16380.
23. J. R. Dilworth and S. J. Parrott, *Chem. Soc. Rev.*, 1998, **27**, 43-55.
24. N. Manav, P. E. Kesavan, M. Ishida, S. Mori, Y. Yasutake, S. Fukatsu, H. Furuta and I. Gupta, *Dalton Trans.*, 2019, **48**, 2467-2478.
25. V. Balzani, S. Campagna, A. Barbieri and I. Ebrary, *Photochemistry and Photophysics of Coordination Compounds II*, Springer-Verlag, Berlin, Germany, 2007.
26. J. V. Caspar, E. M. Kober, B. P. Sullivan and T. J. Meyer, *J. Am. Chem. Soc.*, 1982, **104**, 630-632.
27. J. E. Yarnell, J. C. Deaton, C. E. McCusker and F. N. Castellano, *Inorg. Chem.*, 2011, **50**, 7820-7830.
28. K. A. Wells, J. E. Yarnell, J. R. Palmer, T. S. Lee, C. M. Papa and F. N. Castellano, *Inorg. Chem.*, 2020, **59**, 8259-8271.
29. J. E. Yarnell, K. A. Wells, J. R. Palmer, J. M. Breaux and F. N. Castellano, *J. Phys. Chem. B*, 2019, **123**, 7611-7627.
30. D. S. Tyson, J. Bialecki and F. N. Castellano, *Chem. Comm.*, 2000, 2355-2356.

31. F. N. Castellano, *Acc. Chem. Res.*, 2015, **48**, 828-839.
32. F. N. Castellano, *Dalton Trans.*, 2012, **41**, 8493.
33. D. S. Tyson and F. N. Castellano, *J. Phys. Chem. A*, 1999, **103**, 10955-10960.
34. D. S. Tyson, K. B. Henbest, J. Bialecki and F. N. Castellano, *J. Phys. Chem. A*, 2001, **105**, 8154-8161.
35. C. E. McCusker, A. Chakraborty and F. N. Castellano, *J. Phys. Chem. A*, 2014, **118**, 10391-10399.
36. J. E. Yarnell, C. E. McCusker, A. J. Leeds, J. M. Breaux and F. N. Castellano, *Eur. J. Inorg. Chem. A*, 2016, **2016**, 1808-1818.
37. D. S. Tyson, C. R. Luman, X. Zhou and F. N. Castellano, *Inorg. Chem.*, 2001, **40**, 4063-4071.
38. D. T. Yonemoto, C. M. Papa, C. Mongin and F. N. Castellano, *J. Am. Chem. Soc.*, 2020, **142**, 10883-10893.
39. J. R. Palmer, K. A. Wells, J. E. Yarnell, J. M. Favale and F. N. Castellano, *J. Phys. Chem. Lett.*, 2020, **11**, 5092-5099.
40. M. Mamada, C. Pérez-Bolívar, D. Kumaki, N. A. Esipenko, S. Tokito and P. Anzenbacher Jr, *Chem. Eur. J.*, 2014, **20**, 11835-11846.
41. J. Mizuguchi, *J. Phys. Chem. B*, 2004, **108**, 8926-8930.
42. M. G. Debije, P. P. C. Verbunt, P. J. Nadkarni, S. Velate, K. Bhaumik, S. Nedumbamana, B. C. Rowan, B. S. Richards and T. L. Hoeks, *Appl. Opt.*, 2011, **50**, 163-169.
43. K. I. Kobrakov, N. S. Zubkova, G. S. Stankevich, Y. S. Shestakova, V. S. Stroganov and O. I. Adrov, *Fibre Chem.*, 2006, **38**, 183-187.
44. R. O. Loutfy, A. M. Hor, P. M. Kazmaier, R. A. Burt and G. K. Hamer, *Dyes Pigm.*, 1991, **15**, 139-156.
45. Y. Yang, J. Brückmann, W. Frey, S. Rau, M. Karnahl and S. Tschierlei, *Chem. Eur. J.*, 2020, 17027-17034.
46. S. Garakyaraghi, E. O. Danilov, C. E. McCusker and F. N. Castellano, *J. Phys. Chem. A*, 2015, **119**, 3181-3193.
47. M. J. Frisch, G. W. Trucks, H. B. Schlegel, G. E. Scuseria, M. A. Robb, J. R. Cheeseman, G. Scalmani, V. Barone, G. A. Petersson, H. Nakatsuji, *et al*, *Gaussian 16, Revision A.03*, 2016.
48. C. Adamo and V. Barone, *J. Chem. Phys.*, 1999, **110**, 6158-6170.
49. F. Weigend and R. Ahlrichs, *Phys. Chem. Chem. Phys.*, 2005, **7**, 3297-3305.
50. D. Andrae, U. Häußermann, M. Dolg, H. Stoll and H. Preuß, *Theor. Chim. Acta*, 1990, **77**, 123-141.
51. M. Cossi, G. Scalmani, N. Rega and V. Barone, *J. Chem. Phys.*, 2002, **117**, 43.
52. S. Grimme, J. Antony, S. Ehrlich and H. Krieg, *J. Chem. Phys.*, 2010, **132**, 154104.
53. R. L. Martin, *J. Chem. Phys.*, 2003, **118**, 4775-4777.
54. R. Dennington, T. A. Keith and J. M. Millam, *Gauss View, Ver. 6*, 2016.
55. J. V. Caspar and T. J. Meyer, *J. Phys. Chem.*, 1983, **87**, 952-957.
56. M. R. Gonçalves and K. P. M. Frin, *Polyhedron*, 2017, 20-27.
57. J. E. Yarnell, P. De La Torre and F. N. Castellano, *Eur. J. Inorg. Chem.*, 2017, **2017**, 5238-5245.
58. I. Chakraborty, J. Jimenez, W. M. C. Sameera, M. Kato and P. K. Mascharak, *Inorg. Chem.*, 2017, **56**, 2863-2873.
59. *IUPAC Compendium of Chemical Terminology "Gold Book"*, Blackwell Scientific Publications, Oxford, 2nd edn.
60. A. M. Blanco-Rodríguez, H. Kvapilová, J. Sýkora, M. Towrie, C. Nervi, G. Volpi, S. Záliš and A. Vlček, *J. Am. Chem. Soc.*, 2014, **136**, 5963-5973.
61. F. Deng, J. Blumhoff and F. N. Castellano, *J. Phys. Chem. A*, 2013, **117**, 4412-4419.
62. K. Kalyanasundaram, *J. Chem. Soc., Faraday Trans. 2*, 1986, **82**, 2401.